Lubrication pressure model in a non-negligible gap for fluid permeation through a membrane with finite permeability

Shintaro Takeuchi [1,*] Toshiaki Fukada [2] Shuji Yamada,[1]
Suguru Miyauchi [3] and Takeo Kajishima[1]
[1]*Department of Mechanical Engineering, Osaka University, 2-1 Yamada-oka, Suita-city, Osaka 565-0871, Japan*
[2]*Central Research Institute of Electric Power Industry, 2-6-1 Nagasaka, Yokosuka, Kanagawa 240-0196, Japan*
[3]*Faculty of Engineering, University of Miyazaki, 1-1 Gakuen Kibanadai-nishi, Miyazaki 889-2192, Japan*

(Received 31 March 2021; accepted 13 October 2021; published 5 November 2021)

The membrane permeation of a fluid occurring near the wall is strongly influenced by lubrication because the generated pressure accelerates the fluid passing through the membrane. In the present study, the membrane permeation of a pure fluid driven by the lubrication pressure is modeled for a general wall-membrane geometry to understand the effect of permeability on the permeate flux in a range of wall-membrane gap widths that cannot be treated by the Reynolds lubrication equation. This lubrication effect (referred to as the non-Reynolds lubrication effect) is modeled by including a higher-order pressure component described by the wall-tangential derivative of the local Couette-Poiseuille velocity, and a permeate flux model with the non-Reynolds lubrication effect is developed. The permeation model is validated with a corrugated membrane placed in a two-dimensional parallel channel with a fixed aspect ratio (i.e., the average wall-membrane distance to the longitudinal membrane length) of 0.1. The permeation driven by the lubrication pressure between the membrane and wall is studied by varying the nondimensional permeability. At an infinitesimal permeability, the permeate flux model shows good agreement with the fully resolved numerical simulation owing to the comparable contribution of the Couette and Poiseuille components in the permeation model, whereas the permeation model exhibits a diverging trend at finite permeabilities because the Couette component in the model produces an excessive contribution to the lubrication pressure. However, by applying a simplified renormalization procedure to the Couette component into the lowest-order pressure component, the diverging trend is suppressed and the permeate flux in a finite permeability range is reproduced. The applicability of the renormalization-group permeation model is discussed in terms of the conditions of the wall-membrane gap and permeability range.

DOI: 10.1103/PhysRevFluids.6.114101

I. INTRODUCTION

Mass transfer through permeable membranes is observed in biological environments and industrial applications such as artificial heart-lung apparatuses, microbial culture, and food processing. In dense suspensions of cells or membrane structures, permeable surfaces often form a network of narrow channels in which lubrication occurs. Given that the permeate flux is proportional to

*Corresponding author: shintaro.takeuchi@mech.eng.osaka-u.ac.jp

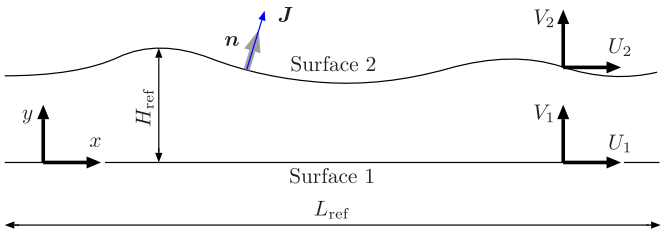

FIG. 1. Schematic of a narrow gap between two moving solid surfaces. The translating velocities of the surfaces are U_i and $V_i (i = 1, 2)$ in the x and y directions, respectively. Surface 2 is assumed to be a permeable membrane, and permeate flux $\boldsymbol{J}$ develops in the surface normal direction $\boldsymbol{n}$. The aspect ratio of the narrow gap is defined with the reference lengths as $\epsilon = H_{\rm ref}/L_{\rm ref}$.

the pressure discontinuity across the membrane with a coefficient called permeability (i.e., a phenomenological model [1,2]), the pressure development caused by lubrication can have a significant impact on the permeation flow through the membrane.

Figure 1 illustrates a schematic of a region between (solid) surfaces where the lubrication occurs. When the surface-to-surface distance is sufficiently small, the Reynolds lubrication equation [3] may be able to describe the lubrication pressure. Tazaki *et al.* [4] mentioned that the order of magnitude of the permeate flux of the solvent driven by the Reynolds lubrication pressure is evaluated as $J^{(\rm Re)}/U \propto \epsilon^{-1}\mathcal{L}$ when the permeability is infinitesimal. Here, $J^{(\rm Re)}$ is the permeate flux, U is the reference velocity, ϵ is the ratio of the gap width to the longitudinal length scale (see Fig. 1), and $\mathcal{L}$ is a nondimensionalized permeability.

However, the applicability of the Reynolds lubrication equation is strongly restricted to negligibly small values of ϵ [5], and lubrication deviating from this geometric condition is widespread [6,7] in dense suspensions. This is because the Reynolds lubrication equation is obtained by only retaining the lowest-order (ϵ^0) effect in the governing equation. In this study, lubrication with a non-negligible value of ϵ is referred to as "non-Reynolds lubrication," and the permeation driven by lubrication pressure is studied in the non-Reynolds lubrication regime for infinitesimal and finite permeabilities. In the following, the models and relevant issues are discussed from the viewpoints classified by a negligible or non-negligible gap (i.e., Reynolds or non-Reynolds lubrication regime) and infinitesimal or finite permeability. These are summarized in Table I.

TABLE I. Models and problems for the cases of negligible or non-negligible gap and infinitesimal or finite permeability.

	Negligible gap ($\epsilon \ll 1$)	Non-negligible gap ($\epsilon \lesssim 1$)
Infinitesimal permeability ($\mathcal{L} \to 0$)	Reynolds lubrication equation (i.e. leading-order equation) ⇓ Lowest-order permeate flux model, Eq. (8)	Non-Reynolds lubrication model (i.e. higher-order model), Eq. (9) consisting of the Poiseuille and Couette components ⇓ Higher-order permeate flux model, Eq. (15)
Finite permeability		Breakdown of the Couette component in the non-Reynolds lub. model, Secs. III C–III D ⇓ RG lubrication model, Eq. (31) (RG: renormalization-group) ⇓ RG permeate flux model

Takeuchi and Gu [8] modeled the pressure in a non-Reynolds lubrication regime as a higher-order (ϵ^2) effect in the form of a wall-tangential variation of the locally constructed Couette-Poiseuille flow (hereafter referred to as the non-Reynolds lubrication model), and Takeuchi *et al.* [7] derived the permeate flux due to the non-Reynolds lubrication. The results showed that the contribution of non-Reynolds lubrication to the permeate flux was estimated to be $J^{(\text{non-Re})}/U \propto \epsilon^1\mathcal{L}$. Their permeate flux model in a non-Reynolds lubrication regime predicted the pressure discontinuity across the membrane [i.e., equivalent to $(J^{(\text{Re})} + J^{(\text{non-Re})})/\mathcal{L}$] and the characteristic distribution of permeation along the membrane (i.e., dimpled profile) in the limit of infinitesimal permeability. However, for finite permeabilities, it was shown that the higher-order term of the lubrication pressure could be larger than the pressure of the lowest-order term (i.e., the pressure that satisfies the Reynolds lubrication equation) [7], indicating the breakdown of the higher-order model and the possibility of unreasonably large permeate fluxes. This may highlight the problems inherent in permeation induced by lubrication pressure at finite permeabilities, and the demand for better higher-order models increases when predicting the pressure and permeate fluxes in the non-Reynolds lubrication regime.

In this study, we propose a lubrication pressure model applicable to a wide range of permeability by including a correction to the above non-Reynolds lubrication model, based on the renormalization-group (RG) method. The RG method was developed to avoid the divergence of the sum of perturbed expansion terms and has been applied to problems in many fields [9–13]. In a typical situation, when a characteristic mode appears in the (perturbation) equation as an inhomogeneous term, a resonance (or secular) term contradicting the boundedness of the solution appears in the simple perturbation expansion, and the perturbation expansion breaks down. Considering that the perturbation terms depend on small parameters, at least a part of the perturbation effect may be renormalized into components (e.g., amplitude and/or phase) that vary only "slowly" in the system [14,15] or are less sensitively related to the system. In this study, the Couette component of the non-Reynolds lubrication model violates the boundedness of the lubrication pressure at finite permeabilities, and by renormalizing the Couette component into the amplitude of the lowest-order component, we propose a model of permeation induced by lubrication pressure applicable to a finite permeability range. For the permeation flow through a moving corrugated membrane, the effect of non-Reynolds lubrication on the permeate flux at finite permeability is revealed by comparing with fully resolved numerical simulations.

II. PROBLEM STATEMENT

To develop a permeation model in a non-Reynolds lubrication regime, we set up a thin corrugated rigid membrane in a two-dimensional parallel channel filled with a single-component fluid, and the membrane is towed at a constant velocity U_0 while maintaining its shape, as illustrated in Fig. 2. The initial position of the corrugated membrane is given as follows:

$$y = h_1(x) = h_0[1 + \delta\cos(kx)],$$

where h_1 is the gap width between the bottom and corrugated plates, $k\ (=2\pi/\ell)$ is the wave number, h_0 is the half channel width, and δ is a parameter between 0 and 1. The corrugation has an infinite extension in the x direction. To express the pressure as a function of the corrugation position in the subsequent section, the prescribed motion of the membrane is presented in the following form:

$$y = h_1(x,t) = h_0\{1 + \delta\cos[k(x - U_0t)]\}. \tag{1}$$

In this study, the results are shown by transforming the frame attached to the moving membrane. The variables observed on this membrane-fixed frame are distinguished by the superscript "$*$", e.g., $h_1(x,t) = h_1^*(x^*) = h_0[1 + \delta\cos(kx^*)]$.

For the geometry of the corrugation and domain, we assume that the amplitude of corrugation $h_0\delta$ is sufficiently small with respect to the half channel width h_0, and h_0 is smaller than the wavelength

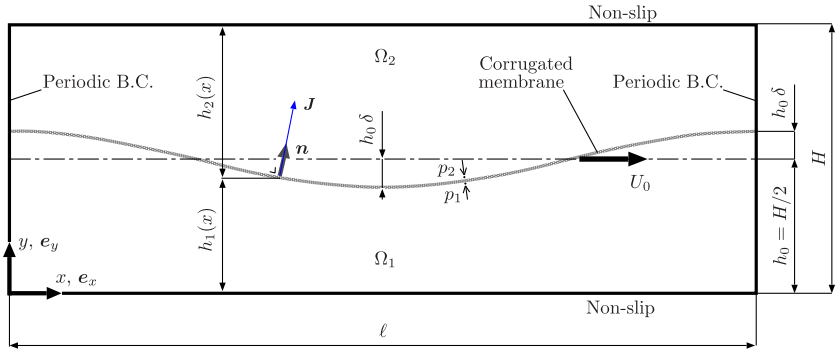

FIG. 2. Corrugated permeable membrane traveling at constant speed U_0 in the $+x$ direction in a parallel channel.

of the corrugation (i.e., $h_0 < 2\pi/k$). The latter condition is equivalent to the aspect ratio ε ($=h_0/\ell = kh_0/2\pi$) being sufficiently small (i.e., $\varepsilon < 1$).

In this study, the developed model for permeation induced by lubrication pressure is compared with fully resolved numerical results. In the numerical simulation, the fluid is an incompressible Newtonian fluid of constant density (ρ) and constant viscosity (μ), and the governing equations of the fluid are the equation of continuity and the Navier–Stokes equation,

$$\boldsymbol{\nabla}\cdot\boldsymbol{u} = 0, \tag{2}$$

$$\frac{\partial \boldsymbol{u}}{\partial t} + \boldsymbol{u}\cdot\boldsymbol{\nabla}\boldsymbol{u} = -\frac{\boldsymbol{\nabla} p}{\rho} + \frac{\mu}{\rho}\nabla^2\boldsymbol{u}, \tag{3}$$

where $\boldsymbol{u}$, t, and p are the velocity, time, and pressure, respectively.

In the present study, the volumetric flux of a pure fluid (i.e., a fluid without any solute) across the membrane is expressed by the following phenomenological model [1,2]:

$$\boldsymbol{J} = L_{\mathrm{p}}[\![p]\!]\boldsymbol{n}, \tag{4}$$

where $\boldsymbol{n}$ is the unit normal vector pointing from the rear side of the membrane Ω_1 to the front side Ω_2, and L_{p} is the permeability. The hydrostatic pressure jump (i.e., discontinuity) across the membrane $[\![p]\!]$ is calculated as $[\![p]\!] = p_1 - p_2$ using the pressure values on the membrane in Ω_1 and Ω_2. In this study, the permeability is nondimensionalized as $\mathcal{L} \overset{\mathrm{def}}{=} L_{\mathrm{p}}\mu/H$, where H is the full channel width (see Fig. 2).

Equations (2)–(4) are numerically solved on a rectangular mesh (i.e., nonconforming to the membrane geometry) by the discrete-forcing immersed-boundary (DF-IB) method provided in Refs. [4,16,17]. To simulate fluid permeation on a rectangular mesh, reproducing the sharpness of the pressure discontinuity across the membrane is critical [18,19]. The DF-IB method described in Refs. [20,21] was developed to reproduce the sharpness in the pressure distribution at a solid surface by handling the mass and momentum conservations even in the immediate vicinity of the solid surface. The present method [4,16,17] solves the problem of permeation by incorporating the pressure discontinuity term into the pressure Poisson equation of the DF-IB method. A brief summary of the numerical method is provided in the Supplemental Material [22].

In this study, the spatial resolution is $H/\Delta = 40$ (except for the cases shown in Fig. 3), where Δ is the grid spacing and the time increment is $\Delta t/(H/U_0) = 8 \times 10^{-6}$. The aspect ratio and Reynolds number are fixed at $\varepsilon = 0.1$ and $\mathrm{Re} = \rho U_0 \ell/\mu = 0.5$, respectively. The other parameters are varied in the following ranges: $\mathcal{L} = 10^{-5}$, 10^{-2}, 10^{-1}, 10^{0} and $\delta = 0.10, 0.25, 0.45, 0.50$, unless specified otherwise.

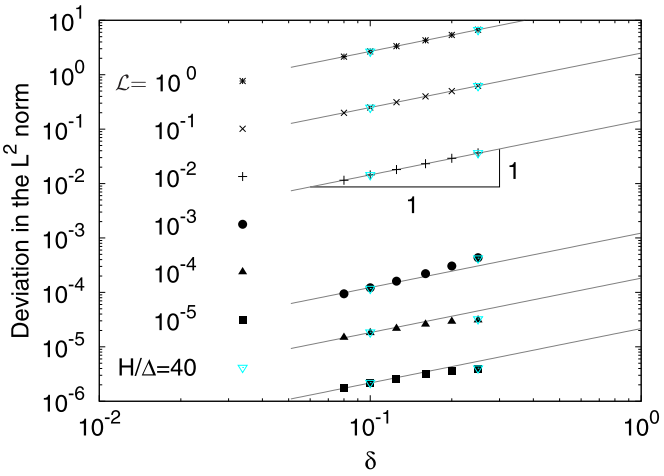

FIG. 3. Deviation in Eq. (8) with respect to the fully resolved numerical result represented in the L^2 norm plotted against δ for the six permeabilities of $\mathcal{L} = 10^{-5}$, 10^{-4}, 10^{-3}, 10^{-2}, 10^{-1}, and 10^{0}. The lines indicate the first-order converging trend. For this graph, the simulation is conducted at a higher spatial resolution of $H/\Delta = 50$, where Δ is the grid spacing. The deviations at the spatial resolution $H/\Delta = 40$ are also plotted with an open symbol for the two δ values employed in the subsequent sections (i.e., $\delta = 0.10$ and 0.25). At both spatial resolutions, the numbers of grid points at the smallest amplitude case are $2h_0\delta/\Delta = 4$, where $2h_0\delta$ is the y displacement of the corrugation.

III. PERMEATE FLUX MODEL AT FINITE PERMEABILITIES

When ε and the Reynolds number $\mathrm{Re} = \rho U_0 \ell/\mu$ satisfy $\varepsilon \ll 1$ and $\varepsilon^2\mathrm{Re} \ll 1$, the pressures in the regions between the membrane and flat walls can be described by the Reynolds lubrication equation (i.e., ε^0th-order equation). Notably, the Reynolds lubrication pressure is uniform in the wall-normal direction, varying only along the x direction. The lubrication pressure reaches a maximum level at the limit of zero permeability ($L_\mathrm{p} \to 0$). However, when ε is not sufficiently small, the pressure in the gap also varies in the wall-normal direction, which is a typical effect of non-Reynolds lubrication for the non-negligible ε. If $\varepsilon \lesssim 1$, $\varepsilon^2 \ll 1$, and $\mathrm{Re} \ll 1$ are satisfied and both the gradient and curvature of the surface profile are small, a lubrication model with a higher-order effect (i.e., the extended lubrication model [8]) is applicable, as will be explained in Sec. III B. Note that regardless of whether in the non-Reynolds or Reynolds lubrication regime, Eq. (4) calculates the permeate flux for a given pressure field.

In this section, by comparing the permeation flow predicted by the non-Reynolds lubrication model with the fully resolved numerical result, we observe a diverging trend of the flux by the model at finite permeabilities, and the suppression of the divergence by a renormalization-group lubrication model is highlighted.

A. Permeate flux model at an infinitesimal permeability

Following Tazaki *et al.* [4], we briefly review in this section the basic model of the permeate flux by the Reynolds lubrication equation under an infinitesimal permeability. Hereafter, the permeate flux under the infinitesimal permeability is referred to as the asymptotic permeate flux. The pressures on the lower and upper sides (Ω_1 and Ω_2, respectively) of the corrugation, $p_1^{(0)}(x,t)$ and $p_2^{(0)}(x,t)$, follow independent Reynolds lubrication equations with no permeation through the membrane. Here, the superscript (0) denotes the lowest-order approximation (i.e., the case described by the Reynolds lubrication equation). The pressure $p_1^{(0)*}(x^*)$ obeys the following Reynolds lubrication

equation:

$$\frac{d}{dx^*}\left[\frac{h_1^{*3}}{12\mu}\left(-\frac{dp_1^{(0)*}}{dx^*}\right)-\frac{U_r^* h_1^*}{2}\right]=0, \tag{5}$$

where U_r is the relative velocity in the x direction between the wall and membrane: $U_r^* = 0 - (-U_0)$. The derivation of this equation is detailed in Ref. [23]. For the present membrane geometry and prescribed motion [Fig. 2 and Eq. (1)], the pressure is given as follows [7]:

$$p_1^{(0)}(x,t) = -\frac{3}{\pi}\frac{P_0}{\varepsilon^2}\frac{\delta}{2+\delta^2}\frac{2+\delta\cos[k(x-U_0t)]}{\{1+\delta\cos[k(x-U_0t)]\}^2}\sin[k(x-U_0t)], \tag{6}$$

where $P_0 = \mu U_0/\ell$. Note that $\varepsilon^{-2}P_0$ is the typical magnitude of the lubrication pressure [23] at the impermeable case ($L_p \to 0$). From the geometric symmetry between Ω_1 and Ω_2 (see Fig. 2) and the one dimensionality of the pressure $p_i^{(0)}$ $(i = 1, 2)$, the pressure in Ω_2 is given as $p_2^{(0)}(x,t) = p_1^{(0)}(x+\pi/k, t)$.

From Eq. (4), the zeroth-order permeate flux is given as follows:

$$J^{(0)*}(x^*) \overset{\text{def}}{=} L_p[\![p^{(0)*}]\!] = L_p\left[p_1^{(0)*}(x^*) - p_2^{(0)*}(x^*)\right]. \tag{7}$$

Substituting Eq. (6) into Eq. (7) and using $h_2(x,t) = h_1(x+\pi/k, t) = 2h_0 - h_1(x,t)$, we obtain the asymptotic permeate flux as follows:

$$J^{(0)}(x,t) = -\frac{24\mathcal{L}U_0}{\pi\varepsilon}\frac{\delta}{2+\delta^2}\frac{\sin[k(x-U_0t)]}{\{1-\delta^2\cos^2[k(x-U_0t)]\}^2}. \tag{8}$$

Here, the permeability L_p is nondimensionalized as $\mathcal{L}$ $(=L_p\mu/H)$.

To study the convergence of the analytical prediction [Eq. (8)] towards the fully resolved numerical result in a wide range of δ, the parameter is varied in the following range: $\delta =$ 0.08, 0.10, 0.12, 0.16, 0.20, and 0.25. Figure 3 shows the converging trend of the deviations in the analytical model [Eq. (8)] with respect to the fully resolved numerical result as a function of δ for different permeabilities. Note that an increased spatial resolution $H/\Delta = 50$ is employed only in this figure to set up a tougher validation condition for Eq. (8), and the cases at the standard spatial resolution $H/\Delta = 40$ are also plotted for reference. The convergence at the first-order rate of δ is observed in the small range of δ for all permeability cases, even though Eq. (8) assumes an infinitesimal $\mathcal{L}$. However, in the range $0.15 < \delta$, the converging trend is not necessarily proportional to δ, suggesting the necessity of a higher-order model, which will be addressed in Sec. III B.

In addition, the graph shows that the deviation level is decreased with decreasing $\mathcal{L}$. However, a large gap is observed in the graph between the data series of $\mathcal{L} = 10^{-3}$ and 10^{-2}, suggesting a nontrivial effect of membrane permeability on the lubrication pressure, which we further address later in Secs. III C and III D.

B. Higher-order adjustment by the extended lubrication model

For a non-negligible value of ε, a higher-order effect must be included by considering the ε^2-order terms in the governing equations. Following the extended lubrication model [8], the non-Reynolds lubrication pressure for the non-negligible ε is decomposed into the base (lowest-order, ε^0) component $p_{\text{Re}}(x)$ and adjusting (higher-order) component $p_{\text{adj}}(x,y)$. Here, p_{Re} is the solution of the Reynolds lubrication equation [i.e., $p_{\text{Re}} = p_i^{(0)}$ $(i = 1, 2)$]; although both p_{Re} and $p_i^{(0)}$ have the same meanings, the notation of $p_i^{(0)}$ is particularly used to specify the region Ω_i $(i = 1, 2)$. In addition, the same symbol $p_i^{(0)}$ is used hereafter for the pressures at arbitrary permeabilities (i.e., both infinitesimal and finite permeabilities); at an infinitesimal $\mathcal{L}$, p_{Re} is as shown in Eq. (6), and p_{Re} at a finite $\mathcal{L}$ will be given in Sec. III D.

Takeuchi and Gu [8] showed that the adjusting component of the pressure can be described as the stress caused by the spatial variation of the locally constructed Couette-Poiseuille flow,

$$p_{\mathrm{adj}}(x, y) = -\mu \frac{\partial (u_{\mathrm{p}} + u_{\mathrm{c}})}{\partial x}, \tag{9}$$

where u_{p} and u_{c} are the Poiseuille and Couette components of the local velocity driven by p_{Re} and the wall movements, respectively,

$$u_{\mathrm{p}} \overset{\mathrm{def}}{=} -\frac{y(h-y)}{2\mu} \frac{d\, p_{\mathrm{Re}}}{dx}, \quad u_{\mathrm{c}} \overset{\mathrm{def}}{=} \frac{y}{h(x)} U_{\mathrm{r}}. \tag{10}$$

Hereafter, p_{adj} is alternatively denoted by $p_i^{(2)}$ $(i = 1, 2)$, indicating that this pressure is the ε^2-order correction to $p_i^{(0)}$. For the boundedness of the lubrication pressure, the ratio of p_{adj} to p_{Re} was obtained as follows [8]:

$$\frac{p_i^{(2)}}{p_i^{(0)}} = \frac{p_{\mathrm{adj}}}{p_{\mathrm{Re}}} \sim \varepsilon^2. \tag{11}$$

We can express the pressure in the non-Reynolds lubrication regime as the sum of the lowest- and higher-order terms as follows:

$$\begin{aligned} p_i^*(x^*, y) &= p_i^{(0)*}(x^*) + p_i^{(2)*}(x^*, y) \quad (i = 1, 2) \\ &= p_{\mathrm{Re}}^*(x^*) + p_{\mathrm{adj}}^*(x^*, y), \end{aligned} \tag{12}$$

and from Eq. (4), the corresponding permeate flux is given as

$$J^{(0+2)*}(x^*) = J^{(0)*} + J^{(2)*}, \tag{13}$$

where

$$J^{(2)*}(x^*) \overset{\mathrm{def}}{=} L_{\mathrm{p}} [\![p^{(2)*}]\!] = L_{\mathrm{p}} \left[p_1^{(2)*}(x^*, y) - p_2^{(2)*}(x^*, y) \right]_{y = h_1^*}. \tag{14}$$

C. Overadjustment of permeate flux

Before we discuss the flux at finite permeability, we first investigate the applicability of the asymptotic flux model $J^{(0+2)*}$. Using Eq. (6), we obtain p_{adj} at $\mathcal{L} \to 0$ from Eq. (9). The explicit form of p_{adj} is not shown here, as it takes a long mathematical form. The corresponding adjusting flux is obtained by Eq. (14) and, finally, the full component of the flux as expressed in Eq. (13) can be given as follows:

$$J^{(0+2)*} = -\frac{24 \mathcal{L} U_0}{\pi \varepsilon} \frac{\delta}{2 + \delta^2} \frac{\sin(kx^*)}{[1 - \delta^2 \cos^2(kx^*)]^2} \left\{ 1 + \frac{2}{3} (\pi \varepsilon)^2 [1 - 4\delta^2 + \delta^2 (5 - 2\delta^2) \cos^2(kx^*)] \right\}. \tag{15}$$

Figure 4 compares the permeate fluxes by the analytical predictions of $J^{(0)}$ [Eq. (8), broken line] and $J^{(0+2)}$ [Eq. (15), solid line] for the two permeabilities $\mathcal{L} = 10^{-5}$ and 10^{-2}. The symbols represent the fully resolved numerical results of the permeate flux. At $\mathcal{L} = 10^{-5}$ [Fig. 4(a)], $J^{(0)}$ underestimates the flux, and the adjustment $J^{(2)}$ compensates the deviation for all the δ cases. Therefore, Eq. (15) is a good approximation of permeate flux in the limit of $\mathcal{L} \to 0$. However, at $\mathcal{L} = 10^{-2}$ [Fig. 4(b)], Eq. (15) largely overestimates the flux compared with the numerical result; the excess of adjustment by the higher-order flux $J^{(2)}$ is hereafter referred to as overadjustment. The departure of the analytical prediction [Eq. (15)] from the fully resolved numerical result is particularly non-negligible with large δ cases, and even a diverging trend is observed at $\mathcal{L} = 10^{-1}$ and 10^0 (not shown here).

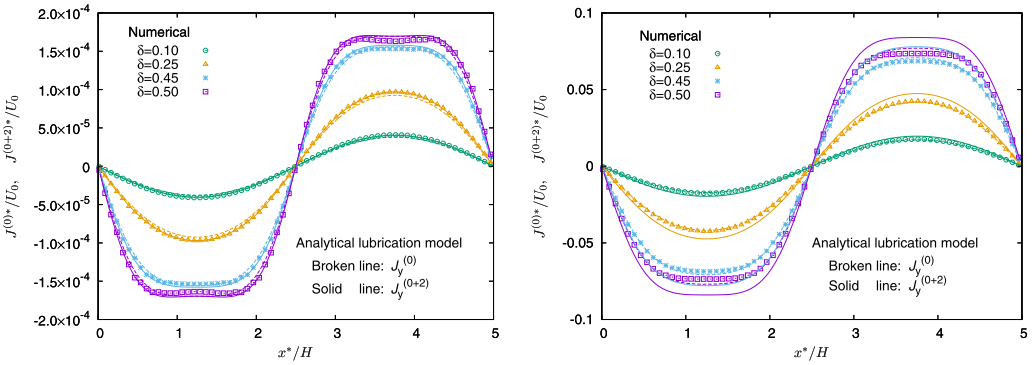

(a) $\mathcal{L} = 10^{-5}$ (b) $\mathcal{L} = 10^{-2}$

FIG. 4. Comparison of the numerical permeate fluxes by the analytical predictions of $J^{(0)}$ [Eq. (8), broken line] and $J^{(0+2)}$ [Eq. (15), solid line] for the two permeabilities $\mathcal{L}\ (= L_p\mu/H) = 10^{-5}$ and 10^{-2}. The symbols represent the fully resolved numerical results of $\boldsymbol{J}\cdot\boldsymbol{n}$ and are plotted every three points.

This overadjustment of the permeate flux by $J^{(2)}$ in the range $\mathcal{L} \geqslant 10^{-2}$ may be partly because Eq. (15) is developed under the assumption of $\mathcal{L} \to 0$. However, a finite value of permeability causes an additional effect, as explained in the next section.

D. Effect of finite permeability on the permeate flux

The contribution of the adjusting flux at a finite permeability is examined through an approximate solution obtained by Fourier decomposition method.

At a finite permeability, the lubrication pressures $p_1^{(0)}$ and $p_2^{(0)}$ are no longer independent, and Eq. (5) is modified to the following form:

$$\frac{d}{dx^*}\left[\frac{h_1^{*3}}{12\mu}\left(-\frac{dp_1^{(0)*}}{dx^*}\right) - \frac{U_0 h_1^*}{2}\right] = -L_p[\![p^{(0)*}]\!], \tag{16a}$$

$$\frac{d}{dx^*}\left[\frac{h_2^{*3}}{12\mu}\left(-\frac{dp_2^{(0)*}}{dx^*}\right) - \frac{U_0 h_2^*}{2}\right] = L_p[\![p^{(0)*}]\!], \tag{16b}$$

assuming that the gradient of the surface profile is sufficiently small (i.e., $\delta\varepsilon \ll 1$). The Fourier decompositions of the pressures,

$$p_1^{(0)*}(x^*) \simeq \frac{P_0}{\varepsilon^2}\sum_{n=0}^{N}[C_n\cos(nkx^*) + S_n\sin(nkx^*)], \tag{17a}$$

$$p_2^{(0)*}(x^*) = p_1^{(0)}(x^* + \pi/k) \simeq \frac{P_0}{\varepsilon^2}\sum_{n=0}^{N}(-1)^n[C_n\cos(nkx^*) + S_n\sin(nkx^*)], \tag{17b}$$

are substituted into Eq. (16), where C_n and S_n $(n = 1, \ldots, N)$ are the coefficients, and N is the number of truncations for the Fourier series. By multiplying $\cos(mkx^*)$ and $\sin(mkx^*)$ to Eq. (16) and integrating in $x^* = [0, 2\pi/k]$, the above coefficients are approximated using the orthogonality of trigonometric functions. With the Fourier-decomposed pressures in Eq. (17), the zeroth-order flux in the Reynolds lubrication regime can be given by Eq. (7). The adjusting component of the pressure is obtained by Eq. (9), and the corresponding (higher-order) flux is obtained by Eq. (14) accordingly.

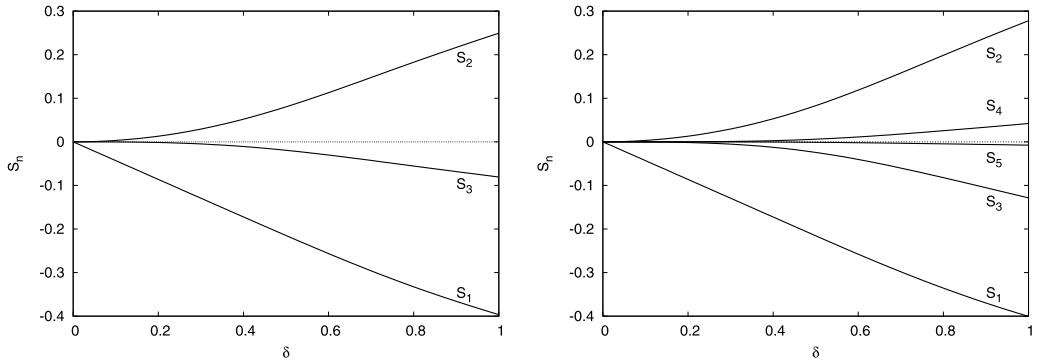

(a) $N = 3$ (b) $N = 5$

FIG. 5. Variation in Fourier sine coefficients of $p_1^{(0)}$ [i.e., Eq. (17)] plotted as a function of δ at $\varepsilon(=h_0/\ell) = 0.1$ and $\mathcal{L}(=L_p\mu/H) = 10^{-2}$ for (a) $N = 3$ [Eq. (18)] and (b) $N = 5$.

The Fourier coefficients at the lowest truncation $N = 1$ are obtained as follows:

$$S_1 = -\frac{12\pi\varepsilon^2\delta}{\pi^2\varepsilon^2(4+9\delta^2)+48\mathcal{L}},$$
$$C_1 = 0.$$

This result indicates that unlike the infinitesimal case of Eq. (6), the pressure is no longer independent of $\mathcal{L}$, which renders the effect of finite permeability.

For a higher truncation case of $N = 3$, the Fourier sine coefficients are obtained as follows:

$$S_1 = \frac{\mathcal{N}_1^{\mathrm{f}\mathcal{L}}}{\mathcal{D}^{\mathrm{f}\mathcal{L}}}, \quad S_2 = \frac{\mathcal{N}_2^{\mathrm{f}\mathcal{L}}}{\mathcal{D}^{\mathrm{f}\mathcal{L}}}, \quad S_3 = \frac{\mathcal{N}_3^{\mathrm{f}\mathcal{L}}}{\mathcal{D}^{\mathrm{f}\mathcal{L}}}, \tag{18}$$

where

$$\mathcal{N}_1^{\mathrm{f}\mathcal{L}} = +12\pi\varepsilon^2\delta[3\pi^2\varepsilon^2(64+48\delta^2+72\delta^4-9\delta^6)+128(2+3\delta^2)\mathcal{L}],$$
$$\mathcal{N}_2^{\mathrm{f}\mathcal{L}} = -12\pi\varepsilon^2\delta^2[3\pi^2\varepsilon^2(48+52\delta^2+15\delta^4)+64(3+\delta^2)\mathcal{L}],$$
$$\mathcal{N}_3^{\mathrm{f}\mathcal{L}} = +12\pi\varepsilon^2\delta^3[12\pi^2\varepsilon^2(8+\delta^2+\delta^4)],$$
$$\mathcal{D}^{\mathrm{f}\mathcal{L}} = \mathcal{D}_0^{\mathrm{f}\mathcal{L}} + \mathcal{D}_1^{\mathrm{f}\mathcal{L}}\mathcal{L} + \mathcal{D}_2^{\mathrm{f}\mathcal{L}}\mathcal{L}^2,$$

and

$$\mathcal{D}_0^{\mathrm{f}\mathcal{L}} = -3(256+192\delta^2+192\delta^4+260\delta^6-105\delta^8)(\pi\varepsilon)^4,$$
$$\mathcal{D}_1^{\mathrm{f}\mathcal{L}} = -16(640+528\delta^2+768\delta^4-97\delta^6)(\pi\varepsilon)^2,$$
$$\mathcal{D}_2^{\mathrm{f}\mathcal{L}} = -6144(2+3\delta^2).$$

The Fourier cosine coefficients are $C_n = 0$ $(n = 1, \ldots, N > 1)$ for the present geometry of the membrane. Although the coefficients at $N \geqslant 5$ are available, the mathematical forms are not presented. Note that according to Eqs. (7) and (17), $J^{(0)}$ with an even value for N $(\geqslant 2)$ is constructed in the same function space as that in the $(N-1)$ case, resulting in no essential difference between the $(N-1)$ and N truncations in Eq. (17).

Figure 5 compares the Fourier sine coefficients for $N = 3$ [Eq. (18)] and $N = 5$ as a function of δ for $\varepsilon = 0.1$ and $\mathcal{L} = 10^{-2}$. From the graph, the effect of S_1 is prominent, and other coefficients are relatively small, particularly in the small range of δ (e.g., $\delta \leqslant 0.25$). Notably, using a higher number of truncations (i.e., $N > 5$), we observe a similar trend. In addition, because $N = 1$ significantly underestimates the flux from our preliminary study, the number of truncations, $N = 3$, is mainly

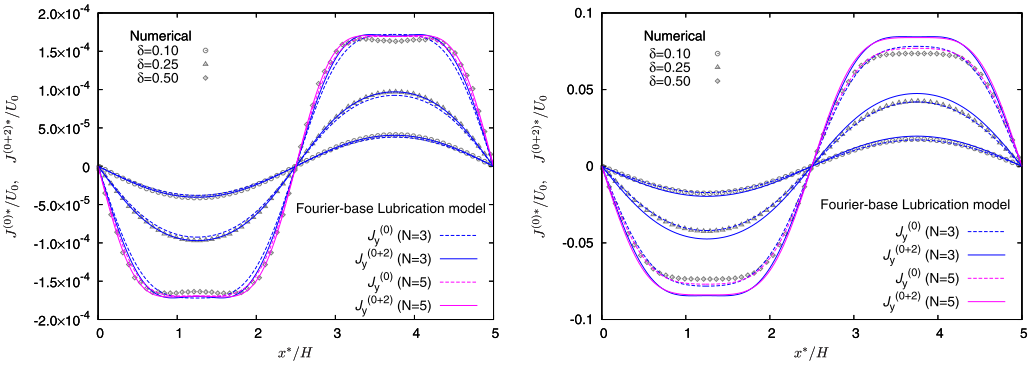

(a) $\mathcal{L} = 10^{-5}$ (b) $\mathcal{L} = 10^{-2}$

FIG. 6. Comparison of numerical permeate fluxes by Fourier decomposition analysis of $J^{(0)}$ [Eq. (17) substituted into Eq. (7), broken line] and $J^{(0+2)}$ [Eq. (14) with Eq. (17), solid line] for the two permeabilities $\mathcal{L}$ $(= L_p\mu/H) = 10^{-5}$ and 10^{-2}. The fully resolved numerical result (symbol) is the same as that in Fig. 4. Case $\delta = 0.45$ is not plotted to avoid overlap with the lines.

employed in the following unless specified otherwise (i.e., the case of $\mathcal{L} = 10^{-5}$ and $\delta = 0.50$). In the following, the mathematical forms of $J^{(0)}$ and $J^{(2)}$ are not presented.

Figure 6 plots the permeate fluxes predicted by the above Fourier decomposition method for $\mathcal{L} = 10^{-5}$ and 10^{-2}. The dashed and solid lines represent $J^{(0)*}$ and $J^{(0+2)*}$, respectively, and the symbol represents the same numerical result as that given in Fig. 4, except that the case of $\delta = 0.45$ is eliminated to avoid excessive overlap with the lines. For both $\mathcal{L} = 10^{-5}$ and 10^{-2}, the profiles of $J^{(0)}$ show that the number of truncations, $N = 3$, gives sufficient accuracy, except for $(\mathcal{L}, \delta) = (10^{-5}, 0.50)$. For this case, the permeate fluxes exhibit the nearly flat profile (or, more precisely, a profile with dimples [7]) at approximately $kx^* = \pi/2$ and $3\pi/2$ (i.e., $x^*/H = 1.25$ and 3.75), and $N = 5$ is necessary to reproduce this characteristic profile. At $\mathcal{L} = 10^{-5}$ [Fig. 6(a)], the contribution of $J^{(2)}$ gives reasonable adjustment to the zeroth-order flux $J^{(0)}$ [Eq. (7)] obtained from Eq. (17). For the case of the finite permeability $\mathcal{L} = 10^{-2}$, the Fourier decomposition method is expected to give a better approximation than Eq. (8), as Eq. (8) is developed under $\mathcal{L} \to 0$. However, the flux model at $N = 5$ for $(\mathcal{L}, \delta) = (10^{-2}, 0.50)$ in Fig. 6(b) gives nearly the same distribution of $J^{(0)}$ as Eq. (8) [Fig. 4(b)]. In addition, when the cases at $N = 3$ and 5 in Fig. 6(b) are compared, the higher Fourier mode ($N = 5$) does not essentially improve the flux distributions. Therefore, $N = 3$ is employed for $\mathcal{L} > 10^{-5}$.

As mentioned with respect to Fig. 4(b), the case of $\mathcal{L} = 10^{-2}$ in Fig. 6(b) also shows the overadjustment by $J^{(2)}$. The deviation trend of $J^{(0+2)}$ from the fully resolved numerical result is evaluated as the difference in the fluxes at $kx^* = \pi/2$ ($x^* = \ell/4 = 1.25H$) and is plotted in Fig. 7 with the square symbol for the four δ values. The result shows that the overadjustment is not suppressed even with the Fourier-based solution, indicating that this is the intrinsic nature of Eq. (9) at a finite permeability. In addition, under predominant permeation at a finite permeability, the lubrication pressure should be even moderated to a value lower than $\varepsilon^{-2}P_0$. Therefore, the overadjustment by $J^{(2)}$ exhibits an inconsistent trend with the expected physical response of the lubrication pressure at large permeabilities, which suggests the necessity of reexamining the pressure in the non-Reynolds lubrication regime. Takeuchi *et al.* [7] reevaluated the orders of magnitude for p_{Re} and p_{adj} at finite permeability as

$$p_{\mathrm{Re}} \sim \frac{V}{L_{\mathrm{p}}} = \frac{\mu V/H}{\mu L_{\mathrm{p}}/H} \sim \frac{P_0}{\mathcal{L}}, \tag{19a}$$

$$p_{\mathrm{adj}} = -\mu \frac{\partial (u_{\mathrm{p}} + u_{\mathrm{c}})}{\partial x} \sim \left(\frac{\varepsilon^2}{\mathcal{L}} + 1 \right) P_0, \tag{19b}$$

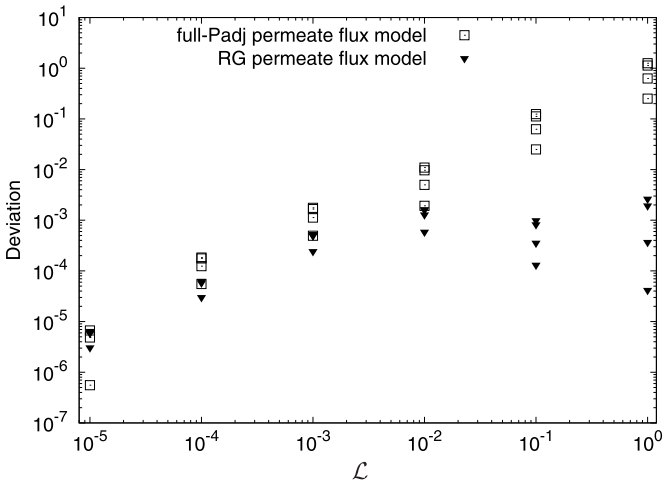

FIG. 7. Deviation of predicted permeate fluxes from the fully resolved numerical result plotted as a function of $\mathcal{L}$. The deviation is taken at $kx^* = \pi/2$ (i.e., $x^* = \ell/4 = 1.25H$) for $\delta = 0.10, 0.25, 0.45$, and 0.50. In the figure, "full-Padj permeate flux model" and "RG permeate flux model" refer to $J^{(0+2)}$ [i.e., the flux with the full components of the $p_{\rm adj}$, Eq. (9) or (22)] and $J^{(0+2)\dagger}$ [i.e., the flux induced by $p^\dagger$, Eq. (31)], respectively.

where V is the reference velocity of the fluid in the transverse direction, and the orders of magnitude of $\mu\partial u_{\rm p}/\partial x$ and $\mu\partial u_{\rm c}/\partial x$ were obtained as $\varepsilon^2 P_0/\mathcal{L}$ and P_0, respectively. Equation (19) shows that while the Poiseuille component $\mu\partial u_{\rm p}/\partial x$ of $p_{\rm adj}$ is in the appropriate ratio to $p_{\rm Re}$ as follows:

$$\frac{\mu\partial u_{\rm p}/\partial x}{p_{\rm Re}} \sim \frac{\varepsilon^2 P_0/\mathcal{L}}{P_0/\mathcal{L}} = \varepsilon^2,$$

the Couette component $\mu\partial u_{\rm c}/\partial x$ can be out of the assumed ratio to $p_{\rm Re}$ at large permeabilities, as shown below,

$$\frac{\mu\partial u_{\rm c}/\partial x|_{y=h}}{p_{\rm Re}} \sim \frac{P_0}{P_0/\mathcal{L}} = \mathcal{L}.$$

Therefore, $p_{\rm adj}$ could become larger than $p_{\rm Re}$ for a large permeability,

$$\lim_{\mathcal{L}\to O(1)} \frac{p_{\rm adj}}{p_{\rm Re}} > 1, \tag{20}$$

which violates the relation of Eq. (11). This changeover of the value of $p_{\rm adj}/p_{\rm Re}$ at large $\mathcal{L}$ directly influences the permeate flux through Eq. (14), which is the cause of the overadjustment.

To remain in the assumed order of magnitude for $p_{\rm adj}/p_{\rm Re}$ as given by Eq. (11), the permeability must be limited in the following range:

$$\mathcal{L} \ll \varepsilon^2. \tag{21}$$

For the present aspect ratio of the corrugated membrane ($\varepsilon = 0.1$), $\mathcal{L} = 10^{-3}$ may be the upper bound for Eq. (9) to be applied without correction to calculate the higher-order component of permeate flux.

E. Renormalization-group (RG) method for the finite permeability cases

The above overadjustment indicates a breakdown of the scale separation (by ε and $\mathcal{L}$) on which asymptotic permeation analysis is based.

However, Eq. (9) still describes the trend of the higher-order pressure near a flat plate ($y = 0$), where the Couette contribution is negligible. Therefore, the decomposition into the contributions of u_p and u_c should be reexamined near the membrane ($y = h$); in particular, the y-proportional term in u_c [see Eq. (10)] requires a detailed investigation. The y-proportional term is recognized as the term that induces a contradicting effect with the boundedness of the lubrication pressure, as shown in Eq. (20). With a correction based on the local flow information, it is expected that Eq. (9) will be improved into a form applicable to the near-membrane region. The form of correction may not be unique, but in the present study, following the philosophy of Chen *et al.* [24,25], the Couette component is renormalized into the lowest-order component.

The standard procedure of the renormalization group (RG) method [24,25] is briefly explained as follows. For the adjusting pressure given by Eq. (9), the variable y in the Couette component is split as $y - \eta + \eta$:

$$\begin{aligned} p &= p_\mathrm{Re} + p_\mathrm{adj} \\ &= p_\mathrm{Re} - \mu\frac{\partial u_\mathrm{p}}{\partial x} - \mu U_\mathrm{r}(y - \eta + \eta)\frac{d(h^{-1})}{dx}, \end{aligned} \tag{22}$$

where η is a renormalization parameter. The effects of $y - \eta$ and $+\eta$ are considered separately; the effect of $+\eta$ is renormalized into the new coefficient $A(\eta)$,

$$p^\dagger = A(\eta)\left[p_\mathrm{Re} - \mu U_\mathrm{r}(y - \eta)\frac{d(h^{-1})}{dx}\right] - \mu\frac{\partial u_\mathrm{p}}{\partial x}. \tag{23}$$

This process is interpreted as follows: considering that U_r ($=U_0$, in the present study) is determined by the boundary condition and this velocity is also directly related to the reference pressure P_0 of p_Re [see Eqs. (6) and (17a)], the effect of $+\eta$ is absorbed into p_Re based on the idea of Ei *et al.* [26] that the integral constant of a nonperturbative solution constitutes a natural coordinate of the invariant manifold. The coefficient A is obtained by solving the renormalization-group (RG) equation $p^\dagger(x, \eta + \Delta\eta) = p^\dagger(x, \eta)$ or $\partial p^\dagger/\partial\eta = 0$, and, finally, η in Eq. (23) is limited to y. The details of this renormalization-group method are explained in Refs. [14,15,24–26].

Before proceeding to the RG equation, we examine the orders of magnitude of the terms in $\partial p^\dagger/\partial\eta$. For the three terms in $\partial p^\dagger/\partial\eta$,

$$\frac{\partial p^\dagger}{\partial\eta} = \frac{dA}{d\eta}p_\mathrm{Re} \tag{24a}$$

$$-\frac{dA}{d\eta}\mu U_\mathrm{r}(y - \eta)\frac{d(h^{-1})}{dx} \tag{24b}$$

$$+A\mu U_\mathrm{r}\frac{d(h^{-1})}{dx}, \tag{24c}$$

we assume that the first and third terms of the right-hand side [Eqs. (24a) and (24c)] balance in magnitude,

$$O\left[\frac{dA}{d\eta}p_\mathrm{Re}\right] = O\left[A\mu U_\mathrm{r}\frac{d(h^{-1})}{dx}\right]\left(= A\frac{P_0}{H}\right). \tag{25}$$

Using Eq. (19a), we obtain the following relation for the order of magnitude of A:

$$\frac{dA}{d\eta} = A\frac{\mathcal{L}}{H}. \tag{26}$$

By substituting Eq. (26) into Eq. (24b), we evaluate the order of magnitude as follows:

$$\frac{dA}{d\eta}\mu U_\mathrm{r}(y - \eta)\frac{d(h^{-1})}{dx} \sim A\frac{\mathcal{L}}{H}\cdot\frac{\mu U_0 H}{\ell H} = \mathcal{L}A\frac{P_0}{H}. \tag{27}$$

In a comparison of Eqs. (25) and (27), Eq. (27) is negligible if the condition $\mathcal{L} \ll 1$ holds. Considering the $\mathcal{L}$ range of Eq. (21), eliminating Eq. (24b) is justified.

Then, the RG equation is simplified to Eq. (24a)+Eq. (24c)=0. In particular, for the present sinusoidal geometry (Fig. 2), because the basis functions of p_{Re} [see Eq. (6) or Eq. (17a) with Fig. 5(a)] and $d(h^{-1})/dx$ are $\sin(kx)$, the RG equation can be solved analytically (leading to essentially the same result as the following treatment). However, to adapt to more general geometries, we propose an even simpler treatment. Considering that the permeate flux is only determined by the pressures on the membrane and the mathematical details of $p^{\dagger}$ in $0 \leqslant y < h$ are not critical, we evaluate p_{Re} and $d(h^{-1})/dx$ in Eq. (24) with the order analysis given by Eq. (19), and thereby obtain the RG equation as Eq. (26). Then, the solution for $A(\eta)$ is as follows:

$$A(\eta) = C \exp\left[\mathcal{L}\frac{\eta}{H}\right], \tag{28}$$

where C is an integral constant. For the determined A, we postulate from Eq. (11) that $p^{\dagger}$ should be of the same order of magnitude as that of p_{Re}, thereby determining C. Now, $p^{\dagger}$ under $\eta \to y$ takes the following form:

$$p^{\dagger} = A(\eta)\big|_{\eta\to y}\, p_{\mathrm{Re}} - \left[A(\eta)(y-\eta)\mu U_{\mathrm{r}}\frac{d(h^{-1})}{dx}\right]_{\eta\to y} - \mu\frac{\partial u_{\mathrm{p}}}{\partial x}, \tag{29}$$

and the order of magnitude is as follows:

$$p^{\dagger} \sim O[A(y)]\frac{P_0}{\mathcal{L}}. \tag{30}$$

This is equated with $O[p_{\mathrm{Re}}]$ $(=P_0/\mathcal{L})$, and the necessary condition is $O[A(y)] = 1$ for any y in $0 \leqslant y \leqslant h(x)$. Considering $\max_{0\leqslant y\leqslant h}|A(y)| = |A(h)|$ for A in Eq. (28), this necessary condition identifies the integral constant as $C = \exp[-\mathcal{L}h/H]$, and the coefficient A is finally obtained as follows:

$$A(y) = \exp\left[-\mathcal{L}\frac{h-y}{H}\right].$$

Substituting this A into Eq. (29), we obtain the renormalized form of the lubrication pressure as follows:

$$p^{\dagger} = \exp\left[-\mathcal{L}\frac{h-y}{H}\right]p_{\mathrm{Re}} - \mu\frac{\partial u_{\mathrm{p}}}{\partial x}. \tag{31}$$

Using the above pressure, the total permeate flux is denoted as $J^{(0+2)\dagger}$. Note that $p^{\dagger}$ includes $\mathcal{L}$, which may be strange in the sense of a (general impermeable) lubrication. We should stress that the pressure in the form of Eq. (31) is applicable only to permeation induced by lubrication pressure.

Figure 8 compares the analytical prediction of $J^{(0+2)\dagger}$ (represented by the red solid line) to the fully resolved numerical result (symbol) for the following range of permeabilities: $\mathcal{L} = 10^{-5}, 10^{-2}, 10^{-1}, 10^{0}$. In addition, we compared the Fourier-based $J^{(0)}$ at $N = 3$ [Eq. (18)] for $\mathcal{L} = 10^{-2}, 10^{-1}, 10^{0}$ and $N = 5$ for $\mathcal{L} = 10^{-5}$, as represented by the black solid line. For $\mathcal{L} = 10^{-5}$ [Fig. 8(a)], the effect of the RG model [Eq. (31)] rather underestimates the permeate flux, suggesting the essential contribution of the eliminated term (i.e., u_{c} component) in the asymptotic range $\mathcal{L} \to 0$. This is reasonable considering that in the limit of $\mathcal{L} \to 0$, both u_{c} and u_{p} terms in p_{adj} take the comparable contributions at $O[\varepsilon^2 P_0]$ [8]. In addition, for the other $\mathcal{L}$ cases [Figs. 8(b)–8(d)], the diverging trends observed in Figs. 4(b) and 6(b) are successfully relaxed, and reasonable agreement with the numerical results is observed for all the corrugation amplitudes δ. This is also confirmed from the deviation of $J^{(0+2)\dagger}$ from the fully resolved numerical result shown in Fig. 7, plotted with the filled triangular symbol.

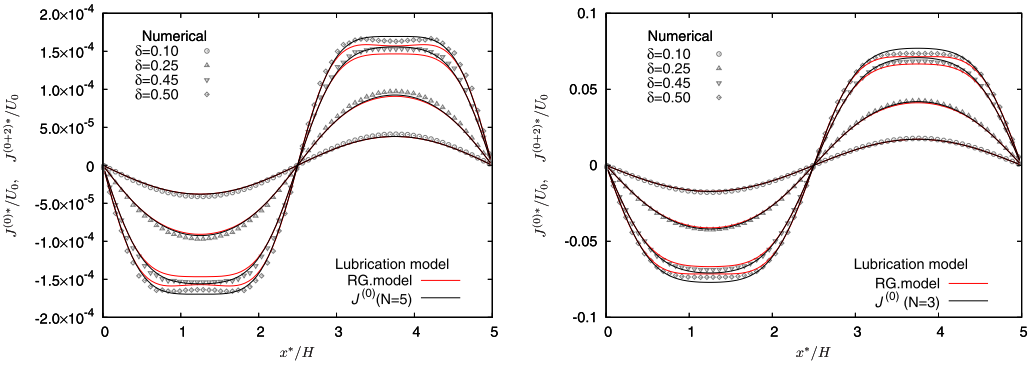

(a) $\mathcal{L} = 10^{-5}$ (b) $\mathcal{L} = 10^{-2}$

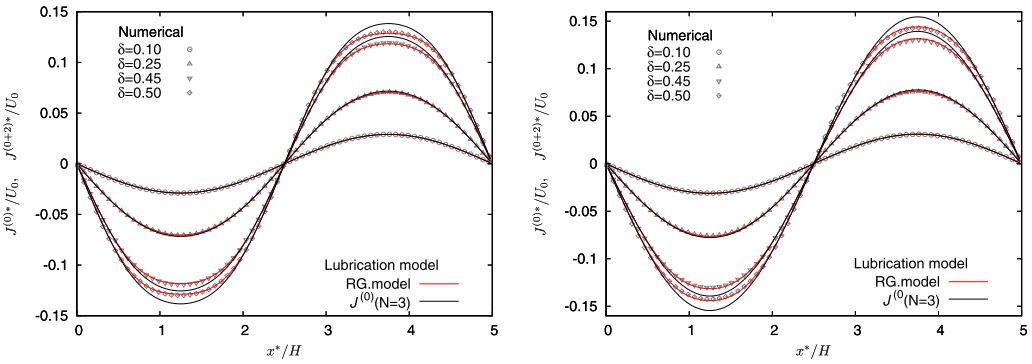

(c) $\mathcal{L} = 10^{-1}$ (d) $\mathcal{L} = 10^{0}$

FIG. 8. Longitudinal (x^*) distribution of the permeate flux for different amplitude parameters δ in the following range of permeabilities: $\mathcal{L} = 10^{-5}, 10^{-2}, 10^{-1}$, and 10^{0}. The Reynolds number is $\mathrm{Re} = \rho U_0 \ell/\mu = 0.5$. The symbols denote the fully resolved numerical results, and the lines are the models for permeation induced by lubrication pressure. "RG model" (red solid line) includes the $p^\dagger$-based higher-order correction [Eq. (31)] with the data of the Fourier-based $J^{(0)}$ (black solid line) at $N = 5$ for $\mathcal{L} = 10^{-5}$, and $N = 3$ [Eq. (18)] otherwise.

It may not be evident that Fig. 8 shows good agreement even out of the expected range for $\mathcal{L}$, given by Eq. (21). This is because, through the renormalization of the u_c component, Eq. (19b) is reevaluated as $\varepsilon^2 P_0/\mathcal{L}$, thereby satisfying the requirement of Eq. (11) for all $\mathcal{L}$s.

The above result suggests that the effect of non-Reynolds lubrication on permeation can be described with the pressure given by Eq. (31).

Finally, the applicable range of the RG flux model and its applicability to more general configurations are summarized. Our analysis showed that the permeate flux driven by the lubrication pressure in the permeability range $\mathcal{L} > \varepsilon^2$ can be described by Eq. (31), whereas Eq. (15) provides a better prediction of the complementary permeability range $\mathcal{L} \leqslant \varepsilon^2$, despite Eq. (31) providing a technically acceptable order of deviation in the small permeability range, as shown in Fig. 7. As the Couette component in p_{adj} showed a diverging trend at a large $\mathcal{L}$, the applicability of the RG flux model [Eq. (31)] to more general flow problems is mainly restricted by the assumptions for the higher-order lubrication pressure model p_{adj}, which are summarized as follows: (i) $\varepsilon^2 \ll 1$, (ii) $\mathrm{Re} \ll 1$, and (iii) $|\partial h/\partial x| \ll 1$ and $|\partial^2 h/\partial x^2| \ll 1$. For the corrugated geometry of the membrane in the present study, the third condition is equivalent to $\delta\varepsilon \ll 1$ [7]; for a more general situation, a weakly undulating membrane forming a relatively narrow wall-membrane gap width may easily satisfy the third condition. Applicability to a flow with a higher Reynolds number is summarized in the Appendix.

IV. CONCLUSION

The higher-order permeate flux of pure fluid through a membrane induced by lubrication pressure was studied at infinitesimal and finite permeabilities by a renormalization-group (RG) method in the range of gap widths wherein the Reynolds lubrication equation was not applicable (i.e., non-Reynolds lubrication regime).

Permeation was assumed to obey a phenomenological model that describes the permeate flux as a pressure discontinuity multiplied by the permeability. The pressure in the non-Reynolds lubrication regime was decomposed into the lowest-order component p_{Re} that satisfies the Reynolds lubrication equation and the higher-order component p_{adj}, and the permeate fluxes induced by the respective pressure components, i.e., the lowest- and higher-order fluxes $J^{(0)}$ and $J^{(2)}$, were obtained. An approximate solution of the Reynolds lubrication equation with permeation condition was obtained by the Fourier-decomposition method, and p_{adj} was constructed as the wall-tangential variation of the Couette and Poiseuille velocity components driven by the moving velocity of the membrane and the gradient of p_{Re}.

The membrane permeation model was validated for a corrugated membrane moving at a constant speed in a parallel channel with impermeable walls. At an infinitesimal permeability, both the Couette and Poiseuille components of p_{adj} exhibited a relatively small order of magnitude with respect to p_{Re}, and the $J^{(2)}$ component provided a reasonable contribution to $J^{(0)}$, leading to good agreement with the fully resolved numerical results at small permeabilities.

However, at finite permeabilities, $J^{(2)}$ provided an excessive adjustment to $J^{(0)}$. This was caused by the diverging effect derived from the Couette component in the non-Reynolds lubrication pressure model, whereas the Poiseuille component in p_{adj} remains in the appropriate order of magnitude regardless of the permeability.

In this study, the Couette component in p_{adj} was renormalized into the lowest-order component p_{Re} by using the RG method to guarantee the boundedness of the lubrication pressure at finite permeabilities. The permeate flux calculated by using the RG lubrication pressure successfully suppressed the diverging component and reasonably predicted the permeate flux in a finite permeability range.

The applicability of the RG permeate flux model is mainly restricted by the applicability of the higher-order lubrication pressure model. Therefore, in addition to the conditions for the Reynolds number and the aspect ratio of the wall-membrane gap to the wall-tangential length scale, the gradient and curvature of the membrane profile must be sufficiently small.

ACKNOWLEDGMENTS

This study was partly supported by Grants-in-Aid for Scientific Research (B) No. 17H03174 and No. 19H02066, Grant-in-Aid for Early-Career Scientists No. 19K20659, and Grant-in-Aid for Challenging Research (Exploratory) No. 20K20972 of the Japan Society for the Promotion of Science (JSPS).

APPENDIX: CASE WITH A LARGER REYNOLDS NUMBER

To investigate the effect of the Reynolds number, a numerical simulation is conducted at $\mathrm{Re} = \rho U_0 \ell/\mu = 5$, although this value is outside the applicable range of the Reynolds number assumed for the model [8]. The longitudinal distributions of permeate flux for the four permeabilities are summarized in Fig. 9. The symbols are the result of the fully resolved numerical simulation at $\mathrm{Re} = 5$, and the lines are the same as those in Fig. 8. On comparing it with Fig. 8, only negligible differences are observed by changing the Reynolds number.

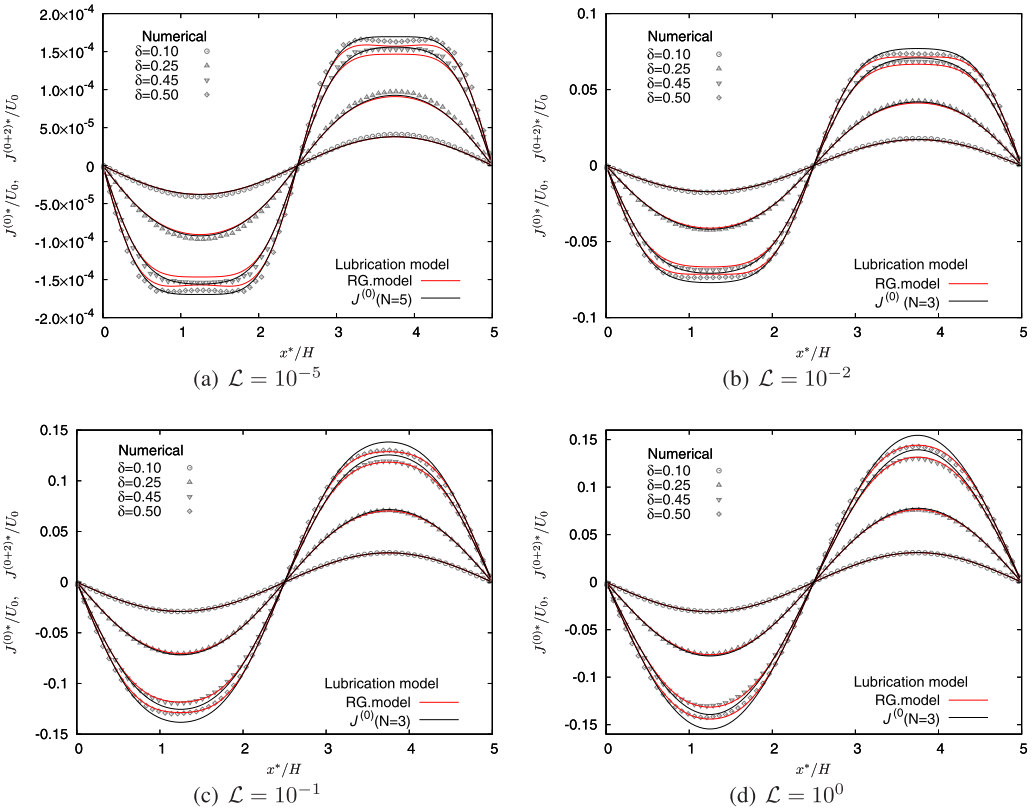

(a) $\mathcal{L} = 10^{-5}$ (b) $\mathcal{L} = 10^{-2}$

(c) $\mathcal{L} = 10^{-1}$ (d) $\mathcal{L} = 10^{0}$

FIG. 9. Longitudinal (x^*) distribution of the permeate flux at $\mathrm{Re} = \rho U_0 \ell/\mu = 5$ for different amplitude parameters δ. The meanings of the symbols and lines are the same as those in Fig. 8.

[1] O. Kedem and A. Katchalsky, A physical interpretation of the phenomenological coefficients of membrane permeability, J. Gen. Physiol. **45**, 143 (1961).

[2] A. Katchalsky and P. F. Curran, *Nonequilibrium Thermodynamics in Biophysics* (Harvard University Press, Cambridge, MA, 1966).

[3] O. Reynolds, On the theory of lubrication and its application to Mr. Beuchamp towers experiments, including an experimental determination of the viscosity of olive oil, Philos. Trans. R. Soc. London **177**, 157 (1886).

[4] A. Tazaki, S. Takeuchi, S. Miyauchi, L. T. Zhang, R. Onishi, and T. Kajishima, Fluid permeation through a membrane with infinitesimal permeability under Reynolds lubrication, J. Mech. **36**, 637 (2020).

[5] J. Gu, M. Sakaue, S. Takeuchi, and T. Kajishima, An immersed lubrication model for the fluid flow in a narrow gap region, Powder Technol. **329**, 445 (2018).

[6] N. Takeishi and Y. Imai, Capture of microparticles by bolus flow of red blood cells in capillaries, Sci. Rep. **7**, 5381 (2017).

[7] S. Takeuchi, S. Miyauchi, S. Yamada, A. Tazaki, L. T. Zhang, R. Onishi, and T. Kajishima, Effect of lubrication in the non-Reynolds regime due to the non-negligible gap on the fluid permeation through a membrane, Fluid Dyn. Res. **53**, 035501 (2021).

[8] S. Takeuchi and J. Gu, Extended Reynolds lubrication model for incompressible Newtonian fluid, Phys. Rev. Fluids **4**, 114101 (2019).

[9] W. D. McComb, *The Physics of Fluid Turbulence* (Oxford University Press, Oxford, 1990).

[10] Y. Nagano and Y. Itazu, Renormalization group theory for turbulence: Assessment of the Yakhot-Orszag-Smith theory, Fluid Dyn. Res. **20**, 157 (1997).
[11] Y. Nagano and Y. Itazu, Renormalization group theory for turbulence: Eddy-viscosity type model based on an iterative averaging method, Phys. Fluids **9**, 143 (1997).
[12] Y. Nambu and Y. Y. Yamaguchi, Renormalization of the long-wavelength solution of Einstein's equation, Phys. Rev. D **60**, 104011 (1999).
[13] P. Kopietz, L. Bartosch, and F. Schuetz, *Introduction to the Functional Renormalization Group* (Springer-Verlag, Berlin, 2010).
[14] T. Kunihiro, A geometrical formulation of the renormalization group method for global analysis, Prog. Theor. Phys. **94**, 503 (1995).
[15] T. Kunihiro, The Renormalization-group method applied to asymptotic analysis of vector fields, Prog. Theor. Phys. **97**, 179 (1997).
[16] S. Takeuchi, A. Tazaki, S. Miyauchi, and T. Kajishima, A relation between membrane permeability and flow rate at low Reynolds number in circular pipe, J. Membr. Sci. **582**, 91 (2019).
[17] S. Yamada, S. Takeuchi, S. Miyauchi, and T. Kajishima, Transport of solute and solvent driven by lubrication pressure through non-deformable permeable membranes, Microfluid. Nanofluid. **25**, 83 (2021).
[18] S. Miyauchi, S. Takeuchi, and T. Kajishima, A numerical method for mass transfer by a thin moving membrane with selective permeabilities, J. Comput. Phys. **284**, 490 (2015).
[19] S. Miyauchi, S. Takeuchi, and T. Kajishima, A numerical method for interaction problems between fluid and membranes with arbitrary permeability for fluid, J. Comput. Phys. **345**, 33 (2017).
[20] N. Sato, S. Takeuchi, T. Kajishima, M. Inagaki, and N. Horinouchi, A consistent direct discretization scheme on Cartesian grids for convective and conjugate heat transfer, J. Comput. Phys. **321**, 76 (2016).
[21] S. Takeuchi, H. Fukuoka, J. Gu, and T. Kajishima, Interaction problem between fluid and membrane by a consistent direct discretization approach, J. Comput. Phys. **371**, 1018 (2018).
[22] See Supplemental Material at http://link.aps.org/supplemental/10.1103/PhysRevFluids.6.114101 for the numerical method used in the present study, which also cites the following paper: T. Ikeno and T. Kajishima, Finite-difference immersed boundary method consistent with wall conditions for incompressible turbulent flow simulations, J. Comput. Phys. **226**, 1485 (2007).
[23] L. G. Leal, *Advanced Transport Phenomena: Fluid Mechanics and Convective Transport* (Cambridge University Press, Cambridge, 2007).
[24] L. Y. Chen, N. Goldenfeld, and Y. Oono, Renormalization Group Theory for Global Asymptotic Analysis, Phys. Rev. Lett. **73**, 1311 (1994).
[25] L. Y. Chen, N. Goldenfeld, and Y. Oono, Renormalization group and singular perturbations: Multiple scales, boundary layers, and reductive perturbation theory, Phys. Rev. E **54**, 376 (1996).
[26] S. Ei, K. Fujii, and T. Kunihiro, Renormalization-group method for reduction of evolution equations; Invariant manifolds and envelopes, Ann. Phys. **280**, 236 (2000).